JOURNAL OF GEOPHYSICAL RESEARCH, VOL. 113, A12102, doi:10.1029/2008JA013589, 2008

Combining remote and in situ observations of coronal mass ejections to better constrain magnetic cloud reconstruction

M. J. Owens[1,2]

Received 8 July 2008; revised 3 September 2008; accepted 9 October 2008; published 10 December 2008.

[1] Determination of the nonradial extent of magnetic clouds (MCs) is vital for two key reasons. First, it affects the amount of "drag" a fast MC experiences and therefore controls the travel time from the Sun to 1-AU, a critical parameter for space-weather prediction. Second, it is vital to estimating the flux content of MCs, which in turn is important for understanding both the formation and eruption of the magnetic flux rope and for determining the role of coronal mass ejections in the heliospheric flux budget and the evolution of heliospheric flux over the solar cycle. In this study, it is demonstrated that the cross-sectional elongation of MCs is poorly constrained by in situ observations of the magnetic field alone. A method for combining remote and in situ observations of ejecta to better determine MC cross-sectional elongation is then outlined and applied to a previously studied event which occurred during the SOHO-Ulysses quadrature of late 1996. The new technique reveals an axial magnetic flux content ~4 times higher than that inferred by a force-free flux rope model fit to the same in situ observations of the magnetic cloud. This event also shows evidence of axial distortion by the structured ambient solar wind.

Citation: Owens, M. J. (2008), Combining remote and in situ observations of coronal mass ejections to better constrain magnetic cloud reconstruction, *J. Geophys. Res.*, *113*, A12102, doi:10.1029/2008JA013589.

1. Introduction

[2] Observations of solar ejecta are predominantly limited to two spatial domains: Remote coronagraph observations of coronal mass ejections (CMEs) in the corona [e.g., *St. Cyr. et al.*, 2000; *Yashiro et al.*, 2005] and in situ observations of their interplanetary manifestations (ICMEs) in the heliosphere [e.g., *Wimmer-Schweingruber et al.*, 2006, and references therein]. Coronagraph observations give a synoptic view of the ejected mass, projected on to the plane of sky (POS) of the observer, while in situ observations directly measure the magnetic field and plasma parameters at a single point within the ejecta as it moves over the fixed observer, yielding a time series that approximates a radial cut through the ICME. Connecting these disparate observations is further complicated by the typical spacecraft positioning, as the majority of multipoint observations have historically been confined to the Earth-Sun line. In such circumstances, the POS projection effect is maximized and CMEs appear as "halo" structures around the occulting disc, making determination of basic CME properties (e.g., velocity and width) difficult without further assumptions [e.g., *Thompson et al.*, 1998]. For this reason, the rarer quadrature observations of ejecta, wherein the angle between the remote observer-Sun line and the in situ observer-Sun line is ~90°, are particularly valuable for understanding the large-scale morphology of solar ejecta [*Lindsay et al.*, 1999]. The new heliospheric imager (HI) instrument on board the STEREO spacecraft may provide serve as a critical link between the coronal and in situ observations, but only a limited number of ejecta have been observed to date [*Harrison et al.*, 2008].

[3] This study demonstrates that the cross-sectional elongation of ejecta is poorly constrained by in situ observations, before outlining new techniques for combining remote and in situ observations of ejecta to better interpret their large-scale structure. The technique is applied to an ejection observed by SOHO and Ulysses during the December 1996 quadrature, as described by *Funsten et al.* [1999], but may prove particularly useful for the STEREO mission when the spacecraft are well separated (~90°). Determination of this cross-sectional elongation of ejecta is vital for two key reasons: Firstly, it is related to the amount of "drag" a fast ejection experiences and therefore controls the travel time from the Sun to 1-AU [*Cargill*, 2004], a critical parameter for space-weather prediction. Secondly, it is vital to estimating the magnetic flux content of ejecta, which in turn is important for understanding both the formation and eruption of the magnetic flux rope, as well as for determining the role of CMEs in the heliospheric flux budget and the evolution of heliospheric flux over the solar cycle [*Owens and Crooker*, 2006; *Owens et al.*, 2007]. The various aspects of ejecta morphology that can be

[1]Center for Space Physics, Boston University, Boston, Massachusetts, USA.
[2]Now at Space and Atmospheric Physics, Blackett Laboratory, Imperial College London, London, UK.

0148-0227/08/2008JA013589$09.00

inferred from remote (section 1.1) and in situ (section 1.2) observations are outlined.

1.1. Remote Observations

[4] Coronagraph observations of CMEs allow estimation of the speed, acceleration, trajectory and width of ejecta, projected on to the observer's plane of sky [*St. Cyr. et al.*, 2000; *Yashiro et al.*, 2005]. For CMEs with trajectories close to the plane of sky (i.e., limb CMEs), such projection errors are negligible. This error, however, increases with the angle between the CME trajectory and the POS. Ejecta which may be encountered in situ by spacecraft in near-Earth space are expected to have trajectories almost perpendicular to the POS (i.e., be directed along the Earth-Sun line). Such events appear as ''halos,'' bright rings around the occulting disc of the coronagraph [e.g., *Thompson et al.*, 1998]. The measured speed of a halo CME is the expansion speed of the ejection, not the speed at which the ejection is moving anti-sunward [e.g., *Schwenn et al.*, 2005]. Furthermore, without additional assumptions and modeling of the observations, such as ''cone models'' of CMEs [e.g., *Zhao et al.*, 2002; *Michalek et al.*, 2003], an estimation of the width of a halo CME is not possible.

[5] A significant fraction of CMEs display a ''3-part structure'' of a bright outer loop, a dark cavity and a bright inner core [*Hundhausen*, 1993]. On the basis of the longitudinal distribution of such ejecta, it has been suggested that this structured morphology is the result of viewing flux rope axes perpendicular to the plane of the sky, whereas unstructured CMEs are flux ropes with axes in the plane of the sky [*Cremades and Bothmer*, 2004].

[6] A number of authors [e.g., *Yurchyshyn et al.*, 2001; *McAllister et al.*, 2001; *Wang et al.*, 2006, and references therein] have looked for correlations between filament and magnetic cloud (MC) orientations, which is possible with observations confined to the Earth-Sun line. In general, only weak correlations have been found, possibly because of a rotation of the filament prior of eruption [*Webb et al.*, 2000]. Such studies, however, have generally relied upon force-free flux rope models to determine the MC orientation, meaning the uncertainty in the magnetic cloud orientation could be very large (see *Riley et al.* [2004] and section 1.3). The techniques outlined in this study should lead to a more accurate determination of magnetic cloud orientation, which will help our understanding of the connection between remote and in situ manifestations of ejecta.

1.2. In Situ Observations

[7] In situ observations of ICMEs allow direct sampling of the plasma, fields and particles at a single point in space. As an ejection travels past the essentially stationary observing spacecraft, a time series of the properties of the ejecta is created. It is important to bear in mind that this time series is only really analogous to a radial cut through the ejection if the ejection is not evolving during its transit: For magnetic clouds, this is rarely the case, with the expansion speed being a significant fraction of the transit speed [e.g., *Owens et al.*, 2005].

[8] For fast ejecta, an interplanetary shock wave is the first in situ signature of an ICME that is encountered, followed by shocked ambient solar wind which piles up in the sheath region bounded by the shock and the ICME leading edge. In this sheath region, pre-existing solar wind structures become compressed into planar structures [*Nakagawa et al.*, 1989] aligned with the ICME leading edge, allowing an estimate of ICME orientation independent of the intrinsic ejecta magnetic fields [*Jones et al.*, 2002]. Further information about the local orientation of the driving ejecta can be obtained from the sheath plasma by examining how the ambient solar wind flow is deflected around the obstacle created by the ICME [*Owens and Cargill*, 2004].

[9] The body of the ICME is identified using a variety of magnetic field, plasma and compositional signatures [e.g., *Wimmer-Schweingruber et al.*, 2006], however, one of the most common indicators of the presence of an ICME is an extended interval of counterstreaming in the suprathermal electrons (CSEs), normally interpreted as ''closed'' field lines which have both ends rooted at the photosphere [*Gosling et al.*, 1987]. Further information about the large-scale structure of ICMEs is generally limited to magnetic clouds, a subset of ICMEs which display a smooth rotation in the magnetic field direction as the ejecta passes over an observing spacecraft [*Burlaga et al.*, 1981; *Klein and Burlaga*, 1982]. This field rotation has been interpreted and modeled as a signature of a flux rope structure [*Goldstein*, 1983; *Burlaga*, 1998; *Lepping et al.*, 1990]. Magnetic clouds have received a great deal of attention for two key reasons: Firstly, they are the drivers of the largest geomagnetic storms [e.g., *Richardson et al.*, 2002], and secondly, the flux rope structure can be exploited to infer properties of their large-scale structure, such as flux content, from the available single-point observations. The next section summarizes current MC-reconstruction techniques.

1.3. Magnetic Cloud Modeling

[10] Initial attempts at reconstructing magnetic clouds used a mathematically simple force-free flux rope model [*Lundquist*, 1950], equivalent to assuming the ICME is cylindrically symmetric with a circular cross-section, at least locally. Models incorporating self-similar expansion, wherein the flux rope cross-section maintains its circular shape but the radius increases with time, have been developed to account for the observed asymmetry in the magnetic field time series [*Marubashi*, 1997]: Failure to take account of MC expansion as it transits over the spacecraft will lead to a significant overestimate of the radial extent of the MC. The force-free flux rope model has proved invaluable for making insights into the morphology of magnetic clouds (e.g., the flux rope forms a loop with both ends attached to the photosphere; *Burlaga* [1998]). However, it has also been shown that the force-free flux rope model is only really applicable when a magnetic cloud is encountered very close to the axis of the flux rope [*Riley et al.*, 2004]. Furthermore, the imposition of a circular cross-section is known to be highly unrealistic, both from observations of shock standoff distance [*Russell and Mulligan*, 2002], and from arguments about propagation in a spherically expanding solar wind: Even if a CME begins life in the low corona as a circular cross-section flux rope, kinematic propagation in spherical geometry will result in a highly elongated cross-section at 1 AU [*Riley and Crooker*, 2004].

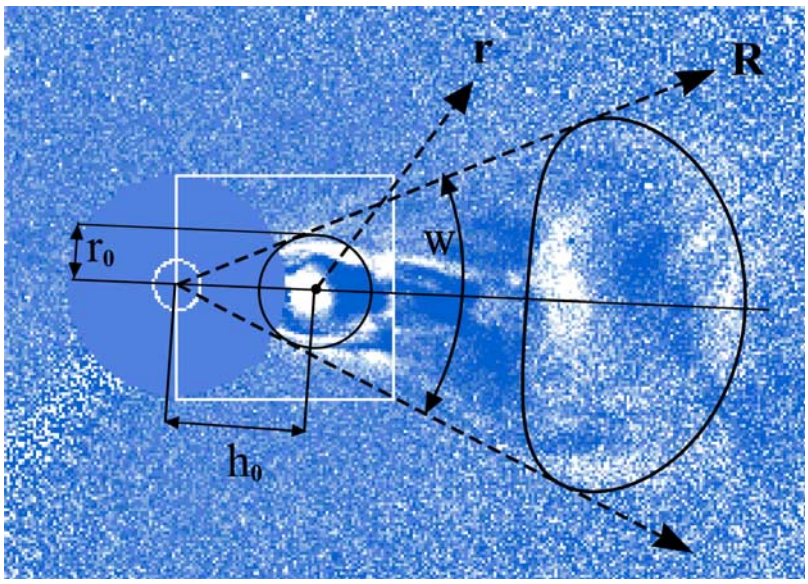

Figure 1. Background: A composition of 2 LASCO C3 difference images. Inside (outside) the white box is 04:13 (10:55) UT 22 December 1996. If CMEs are assumed to be approximately symmetric, LASCO observations of limb CMEs can be used to constrain CME width (W). Foreground: The geometry used by the magnetic cloud model of *Owens et al.* [2006]. The cross-section of the initial force-free flux rope is shown as a black circle inside the white box. It has a radius r_0, is located at a height h_0, and subtends an angular width of W. This flux rope moves subject to a speed V_{SW}(V_{EXP}) in the R(r) direction, meaning at some later time, the flux rope cross-section is given by the black noncircular curve on the right.

[11] Attempts have been made to relax the force-free assumption, normally by allowing the flux rope cross-section to take an arbitrary shape [e.g., *Hu and Sonnerup*, 2001; *Hidalgo et al.*, 2002; *Mulligan and Russell*, 2001]. While the greater flexibility allows a better "fit" in terms of reducing the mean-square-error between the model and observed magnetic field time series, it is not clear that a more accurate reconstruction of the large-scale structure is obtained [*Riley et al.*, 2004], as the extra free parameters leave the fitting process even less constrained. Furthermore, the cross-sectional elongation still remains routinely underestimated [*Riley et al.*, 2004].

[12] *Owens et al.* [2006] and *Owens* [2006] took a different approach in moving away from the force-free approximation, allowing an initially circular cross-section flux rope in the low corona to distort only in a manner consistent with a spherical solar wind expansion, similar to the conceptual picture put forward by *Riley and Crooker* [2004]. By imposing constrains consistent with the known physics of the system, it is hoped the fitting process is better constrained.

[13] The foreground of Figure 1 shows the geometry used in the magnetic cloud model of *Owens et al.* [2006]. The cross-section of the initial force-free flux rope is shown as a black circle inside the white box. It has a radius r_0, is located at a height h_0 and subtends an angular width of W, given by:

$$W = \arctan\frac{r_0}{h_0} \tag{1}$$

For the purposes of fitting a flux rope model to data, h_0 is typically set to a constant value ($2R_S$) and r_0 is varied to allow different CME angular widths.

[14] This force-free flux rope is then kinematically evolved by two velocities: anti-sunward propagation of the flux rope in the R direction at a speed V_{SW}, and axis-centered expansion in the r direction at a speed V_{EXP}. In order to maintain a constant angular width, as is observed in the LASCO field of view, only the component of V_{EXP} along the R direction is considered. See the work of *Owens et al.* [2006] for more detail.

[15] The ratio of V_{EXP} to V_{SW}, denoted A, affects the cross-sectional shape of the resulting magnetic cloud and determines the asymmetry in the magnetic field time series (as the magnetic cloud will continue to expand as it travels past an observing spacecraft). The helicity, H, of the flux rope can be take of value of either +1 or −1, and determines the sense of rotation of the magnetic field relative to the axial field. To make comparisons with time series obtained by in situ measurements, three more parameters are required to characterize the orientation and position of the magnetic cloud relative to the observing spacecraft. These are Y_0, the closest approach of the spacecraft to the flux-rope axis and ϕ_{AXIS} (θ_{AXIS}), the angle the flux rope axis makes in the ecliptic/R-T plane (out of the ecliptic/R-T plane), for GSE/RTN coordinates.

[16] *Owens et al.* [2006] fit the model time series to the observed magnetic field components, requiring one additional parameter to describe the axial field strength of the flux rope (B_0). This study adopts the approach of *Burlaga* [1998], minimizing the difference between the model time

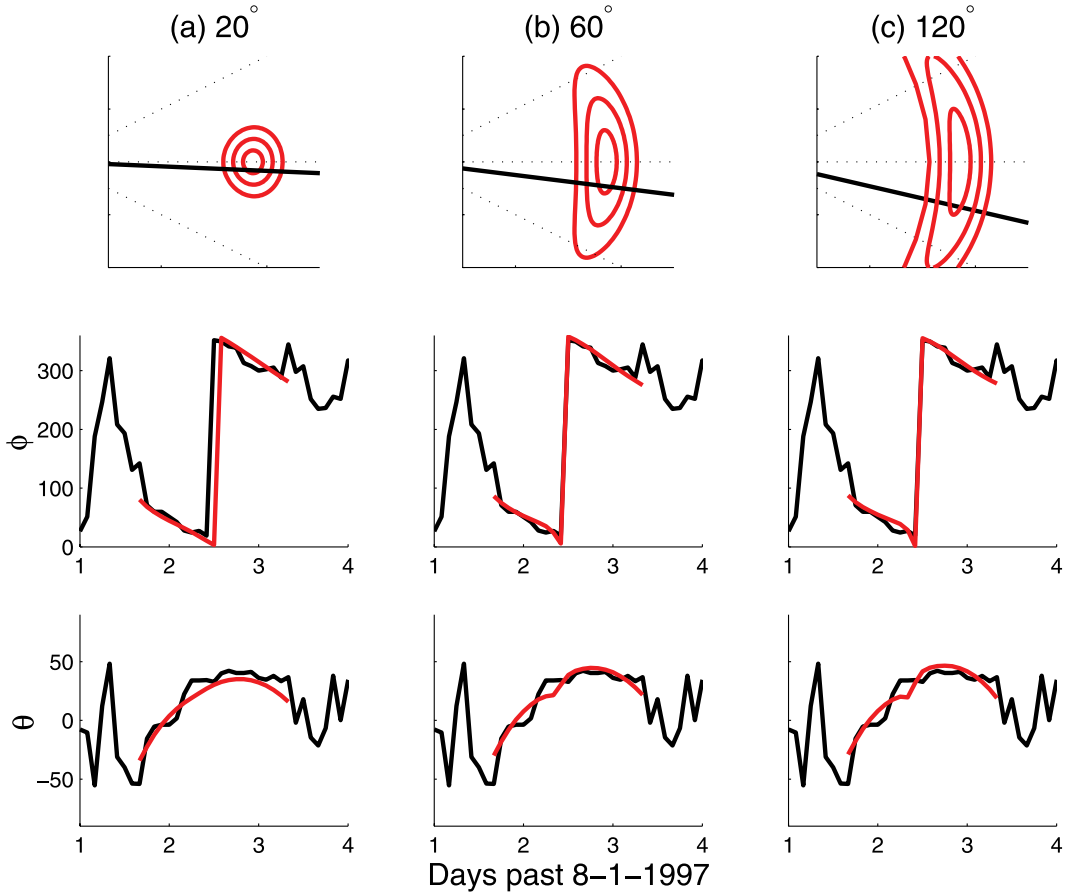

Figure 2. The cross-sectional elongation of magnetic clouds is poorly constrained by in situ observations alone, as demonstrated by three different magnetic cloud model fits to the January 1997 magnetic cloud observed by Ulysses. The first row shows the cross-section of the magnetic cloud models, the third row shows the observed (black) and model (red) time series of the magnetic field angles. The parameters used to characterize the three model magnetic clouds are identical, except for the angular width, which is varied from (a) 20, (b) 60, to (c) 120°. Despite the differing cross-sectional extents of the magnetic clouds, the resulting magnetic field time series are almost identical, demonstrating that elongation is poorly constrained on the basis of in situ data.

series and the observed magnetic field angles (i.e., field magnitude is not included). Thus a value for B_0 is not required and the number of free parameters of the fit is reduced. From this first minimization, the values for six free parameters are obtained:

[17] 1. H, the helicity of the flux rope, either +1 or −1

[18] 2. r_0, which determines the angular width of the flux rope cross-section, W

[19] 3. A, which determines the expansion of the flux-rope

[20] 4. ϕ_{AXIS} and θ_{AXIS}, which determine the orientation of the flux rope axis

[21] 5. Y_0 which determines the point of intersection of the spacecraft relative to the flux rope axis.

[22] Once these parameters are determined, B_0 can then be independently obtained by a second minimization to the magnetic field components.

[23] In the next section, this kinematically distorted flux rope model is used to demonstrate that the cross-sectional elongation of magnetic clouds is poorly constrained on the basis of in situ observations.

2. Magnetic Cloud Elongation

[24] Figure 2 shows three different magnetic cloud model fits (using the model of *Owens et al.* [2006]) to the January 1997 magnetic cloud observed by Ulysses, used here for demonstration purposes (see section 3.3 for more detail about this particular magnetic cloud and of the fit parameters used). The first row show the cross-sections of the model magnetic clouds, the second and third rows show the observed (black) and model (red) angles of the magnetic field. The parameters used to define the three model magnetic clouds (helicity, axis orientation, cloud expansion, magnetic field strength and point of spacecraft intersection) are all identical except for the angular width the initial flux rope subtends with respect to the Sun. This parameter is varied from (1) 20, (2) 60 to (3) 120°, greatly increasing the

cross-sectional elongation of the resulting magnetic clouds (note that Figure 2a is essentially a force-free flux rope). Despite the large differences in the cross-sectional shapes of the fitted flux ropes, the resulting model magnetic field time series are almost indistinguishable. Thus it is difficult to see how any model or technique could reliably determine the nonradial extent of the flux rope on the basis of in situ observations of the magnetic field alone. While this is unlikely to greatly effect estimates of magnetic cloud orientation (see section 3.3), it will have a significant effect on estimates of ejecta properties such as magnetic flux content and solar wind drag.

[25] As cross-sectional elongation is poorly constrained by in situ observations alone, it is necessary to incorporate additional information from coronagraph observations of the CME width into magnetic cloud reconstruction. In the model of *Owens et al.* [2006], a value for the CME width is required to make an initial estimate of the free parameter r_0. They set the initial value of r_0 in accordance with an angular width of 60°, equal to typical CME widths observed by LASCO [*Yashiro et al.*, 2005]. Although this parameter is then allowed to vary so as to minimize the difference between the model and observed magnetic field time series, in practice this simply results in the "best fit" estimate of magnetic cloud elongation being set by the choice of initial value, as nonradial elongation does not greatly effect the magnetic field time series (as shown in Figure 2).

[26] As coronagraph observations of Earth-directed CMEs often take the form of bright "halo" structures surrounding the occulting disc [e.g., *Thompson et al.*, 1998; *Webb et al.*, 2000], there must exist a degree of symmetry to ejecta. Thus it may be safe to assume the coronagraph-measured angular width of a CME occurring near the solar limb should be independent of the CME's orientation (see, however, section 4), a feature exploited by "cone" models of CMEs [e.g., *Zhao et al.*, 2002; *Michalek et al.*, 2003]. It is further assumed that this angular width is maintained throughout the ejecta's journey: LASCO observations of CMEs out to $30R_S$ suggest this is a reasonable assumption [*Yashiro et al.*, 2005], as does the predominantly radial solar wind velocity observed in the body of ICMEs (though large nonradial flows can occur by the deflection of ambient solar wind up- and down-stream of fast ejecta). With these assumptions, the measurement of the angular width of a limb CME can be taken as a direct measurement of parameter W, removing the free parameter r_0 from the magnetic cloud reconstruction process. In the next section this scheme is demonstrated using observations of an ejection made during the quadrature of SOHO and Ulysses in late 1996.

3. Case Study: The December 1996 SOHO-Ulysses Quadrature

[27] In this section, the previously documented quadrature observation of a CME-ICME event is used to demonstrate how remote and in situ observations may be combined to better understand the morphology of ejecta. From December 1996 to January 1997, Ulysses was in approximate quadrature with the Earth-Sun line, situated close to the west limb of the Sun, at a heliocentric distance of ~4.7 AU and a heliolatitude of around 19°. During this period, a number of limb CMEs observed by LASCO can be directly associated with ICMEs later observed by Ulysses [*Funsten et al.*, 1999].

3.1. SOHO Observations

[28] In late December 1996, LASCO observed CMEs at a rate of approximately 1 per day, all off the west limb of the Sun, and with apparent trajectories close to the ecliptic plane [*Yashiro et al.*, 2005]. The majority of the CMEs were small and/or faint in appearance, but the CME occurring at 21:30 UT on 21 December was unique for this time period, in that it was both bright and displayed the classic 3-part structure [*Hundhausen*, 1993]. Using a second-order fit to the LASCO height-time measurements, *Yashiro et al.* [2005] estimated the speed of the CME leading edge to be ~500 km/s near the edge of LASCO's field of view. Ballistic propagation to 4.73 AU, Ulysses' position during this period requires a travel time of ~16.4 days, putting the ICME leading edge at Ulysses early on 7 January 1997. A linear fit to the height-time plot gives a speed of 347 km/s, which puts the ejecta at 4.73 AU early on 14 January 1997. These estimates bound the actual observed arrival time of a magnetic cloud at Ulysses (see section 3.2), suggesting a strong correspondence between the CME and ICME, as reported by *Funsten et al.* [1999].

[29] *Yashiro et al.* [2005] determined the angular width of the 21 December CME to be 72°. This particular ejection was also cataloged by O.C. St Cyr (see the Version 2 lists available at ftp://lasco6.nascom.nasa.gov/pub/lasco/status/) as a "nice 3-part [CME] w/loop arcade." The background images of Figure 1 show two separate LASCO C3 difference images of this CME: Inside (outside) the white box is the image from 04:13 (10:55) UT 22 December 1996. The interpretation of *Cremades and Bothmer* [2004] of a structured CME (i.e., a bright outer loop bounding a dark cavity and a bright inner core) suggests the flux rope within the ejection had its axis perpendicular to the plane of the sky.

3.2. Ulysses Observations

[30] Figure 3 shows 5-minute averages of the heliospheric magnetic field (first three rows) and solar wind plasma (last 5 rows) measured by Ulysses from 7 to 14 January 1997. The vector data is shown in a spacecraft-centered coordinate system, with X pointing toward the Sun, Y given by $\Omega \times X$ where Ω is the north-pointing solar rotation, and Z completing the right-handed set. Thus XYZ are related to the more commonly used RTN coordinate system by $X = -R$, $Y = -T$ and $Z = N$. This XYZ coordinate system is used to follow the conventions used by the magnetic cloud model of *Owens et al.* [2006], which was developed primarily for use on GSE data, wherein X_{GSE} points toward the Sun.

[31] Ulysses observed an interplanetary forward shock at ~0:00 UT on the 9 January 1997, shown as the left-most vertical red line in Figure 3. A hot, dense sheath region followed the shock for approximately 16 hours, which exhibited relatively strong and ordered nonradial solar wind flow deflections. Averaging over the whole sheath region gives flows of approximately equal magnitudes (~30km/s) of the deflected flow in Y and $-Z$ directions. The magnetic field in this sheath region was highly ordered into planar structures, suggesting a systematic pile-up of pre-existing solar wind structures [*Jones et al.*, 2002]. Figure 4 shows

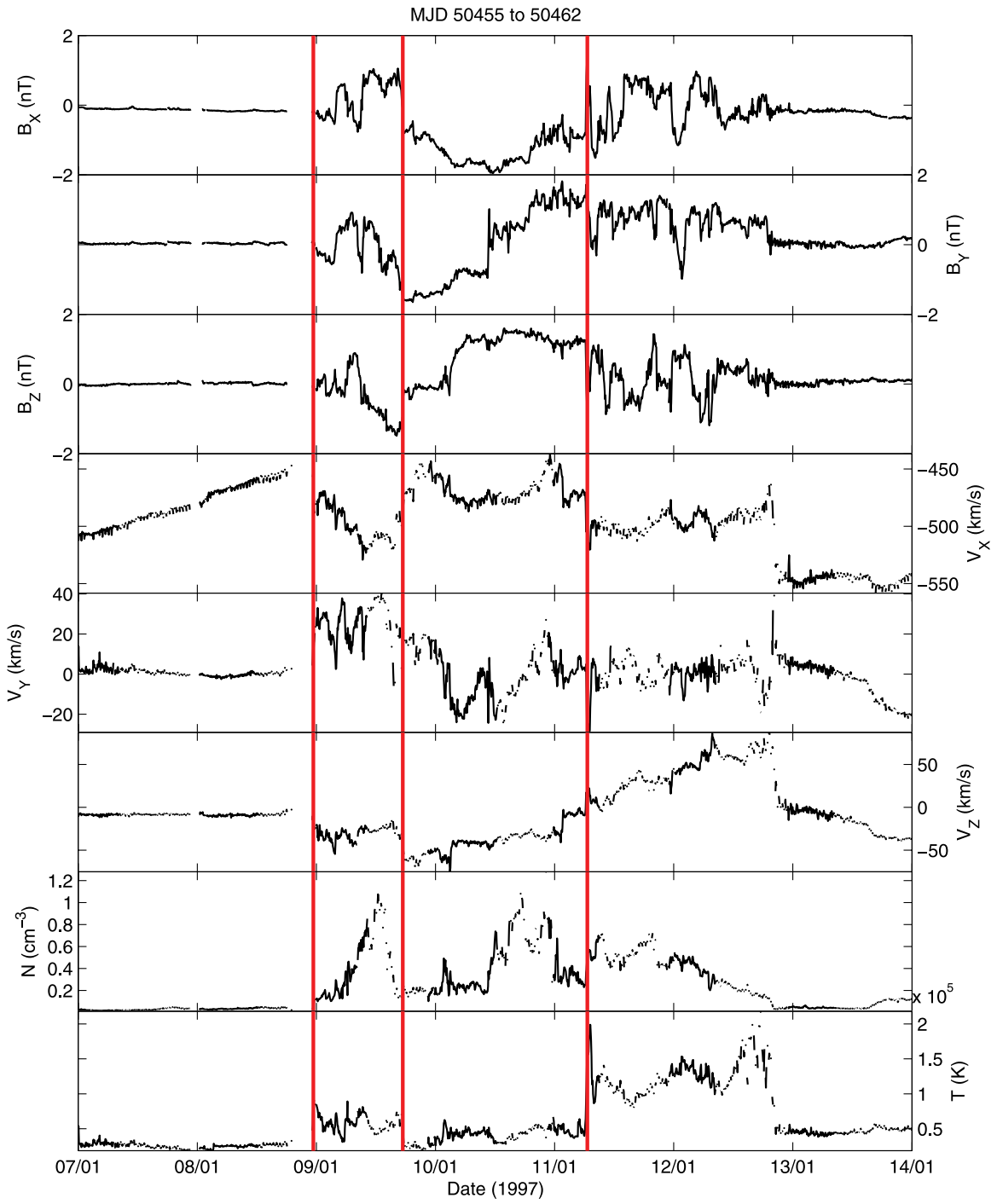

Figure 3. The solar wind observed by Ulysses from 7 to 14 January 1997. The first three rows show the components of the magnetic field. The *X* direction points toward the Sun, *Y* is the cross-product of *X* and the solar rotation axis, and *Z* is completing the right-handed set. The last five rows show the solar wind plasma. From left to right, the red vertical lines show the shock arrival and the magnetic cloud leading and trailing edges.

the angles of the magnetic field in the sheath region: θ is the angle out of the *XY* plane and ϕ is the clock-angle in the *XY* plane, from +*X* through +*Y*. Minimum variance analysis [*Sonnerup and Cahill*, 1967] reveals that the magnetic field lies in a plane with a normal orientation given by [0.63 −0.47 0.62], shown by the red curve. The leading edge orientations suggested by the deflected solar wind flow and the planar magnetic structuring are consistent with each other.

[32] Late on 9 January 1997, Ulysses entered into the ejection material itself, bounded by the two right-most vertical red lines in Figure 3. The ICME is characterized by a smooth magnetic field rotation and low proton temperature of a classic magnetic cloud [*Burlaga et al.*, 1981],

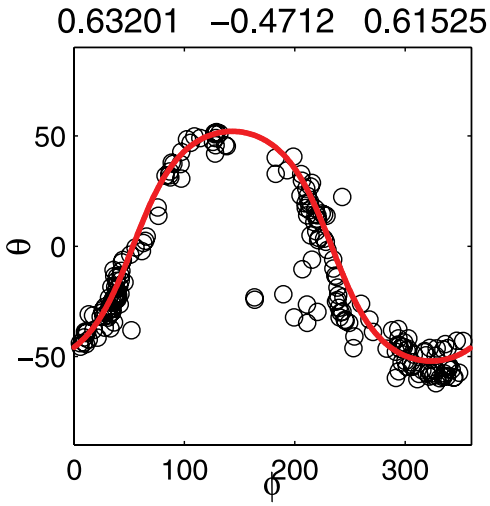

Figure 4. The angles of the magnetic field in the sheath region preceding the January 1997 ICME. The field is highly planar, with a plane normal given by [0.63 −0.47 0.62], shown by the red curve.

which lasts for approximately a day and a half. The mean speed within the magnetic cloud is ∼460 km/s. Assuming constant speed, the leading edge of this structure would have left the Sun ∼18 days earlier, suggesting a launch date of early 22 December 1996, and providing further confidence that is indeed the interplanetary manifestation of the limb CME described in section 3.1. Thus it is assumed that the nonradial extent of the magnetic cloud is equal to the angular width of the source CME (i.e., 72°).

3.3. Flux Rope Fits

[33] Flux rope models are now used to reconstruct the global morphology of the magnetic cloud when it encountered Ulysses, in particular, highlighting the different estimates of magnetic flux which arise from the various models.

[34] Force-free flux rope fits to the magnetic field time series are still the most commonly used technique for magnetic cloud reconstruction. Fitting such a model to spacecraft data requires the helicity of the flux rope (either +1 or −1), the two angles of the axis orientation, the axial field strength and the point of interception of the spacecraft to be free parameters of the fit. Table 1 lists the basic parameters derived from a force-free flux rope fit to the observed magnetic field time series. H is the handedness of the field rotation, $\phi_{\rm AXIS}$ and $\theta_{\rm AXIS}$ describe the orientation of the flux rope axis, Y_0 is the closest approach of the spacecraft to the axis (expressed as a fraction of the cross-sectional extent), A describes the expansion of the flux rope (as a ratio of expansion to transit speed), B_0 is the axial field strength, e is the elongation of the cross-section (as a ratio of the nonradial to radial extent) and Φ is the inferred total axial flux content of the MC.

[35] Fits of a kinematically distorted flux rope model to the observed magnetic cloud magnetic fields are also performed, in the same manner as that of *Owens et al.* [2006], but with the cross-sectional extent of the flux rope imposed by specifying a CME angular width. As with an expanding force-free flux rope model, this leaves five remaining free parameters: The helicity of the flux rope (either +1 or −1), the two angles of the axis orientation, the expansion speed of the cloud and the point of interception of the spacecraft. These are obtained by minimizing the MSE between the observed and model magnetic field angles. A second minimization of the MSE between the observed and model magnetic field components is performed to determine the axial field strength of the flux rope. Table 1 shows the results of fitting the kinematically distorted flux rope model with angular width constrained at 30° and 72°. The latter value is the width of the associated limb CME observed by LASCO, and the associated model fit is shown in Figure 5.

[36] The axis orientations derived from the force-free and the kinematically distorted flux rope fits are in good agreement, as might be expected for a magnetic cloud encounter close to axis [*Riley et al.*, 2004]. Furthermore, these axis orientations agree well with the orientation of the planar magnetic structures and deflected solar wind flows observed in the sheath. Estimates of the cross-sectional elongation, however, are very different for the different model fits, ranging from 1 for the circular cross-section imposed by the force-free assumption, up to ∼5 for the kinematically distorted flux rope with the LASCO-determined CME width of 72° imposed. This results in the factor 4 difference in the estimated axial flux.

[37] Figure 5 shows a summary of the best-fit to the magnetic cloud, using the kinematically distorted flux rope model with the LASCO-derived CME width. The top left panel shows the shape of the magnetic cloud cross-section, the three smaller panels surrounding it show the axis orientation. The bottom two panels on the left show the time series of the observed (black) and model (red) mag-

Table 1. A Summary of the Basic Parameters of the Magnetic Cloud Observed by Ulysses, as Inferred Using Different Magnetic Cloud Models[a]

Model	H	θ_{AXIS} (deg)	ϕ_{AXIS} (deg)	Y_0	A	B_0 (nT)	e	Φ (Wb)
Force-free flux rope *Owens et al.* [2006]	+1	35	208	−0.1	...	2.1	1	4.8×10^{11}
Width = 30°	+1	40	205	−0.25	0.15	2.3	1.8	7.8×10^{11}
Width = 72°	+1	40	205	−0.25	0.15	2.3	5.2	1.9×10^{12}

[a] H is the handedness of the field rotation, ϕ_{AXIS} and θ_{AXIS} describe the orientation of the flux rope axis, Y_0 is the closest approach of the spacecraft to the axis (expressed as a fraction of the cross-sectional extent), A describes the expansion of the flux rope (as a ratio of expansion to advection speed), B_0 is the axial field strength, e is the elongation of the cross-section (as a ratio of the nonradial to radial extent), and Φ is the inferred total axial flux content of the MC.

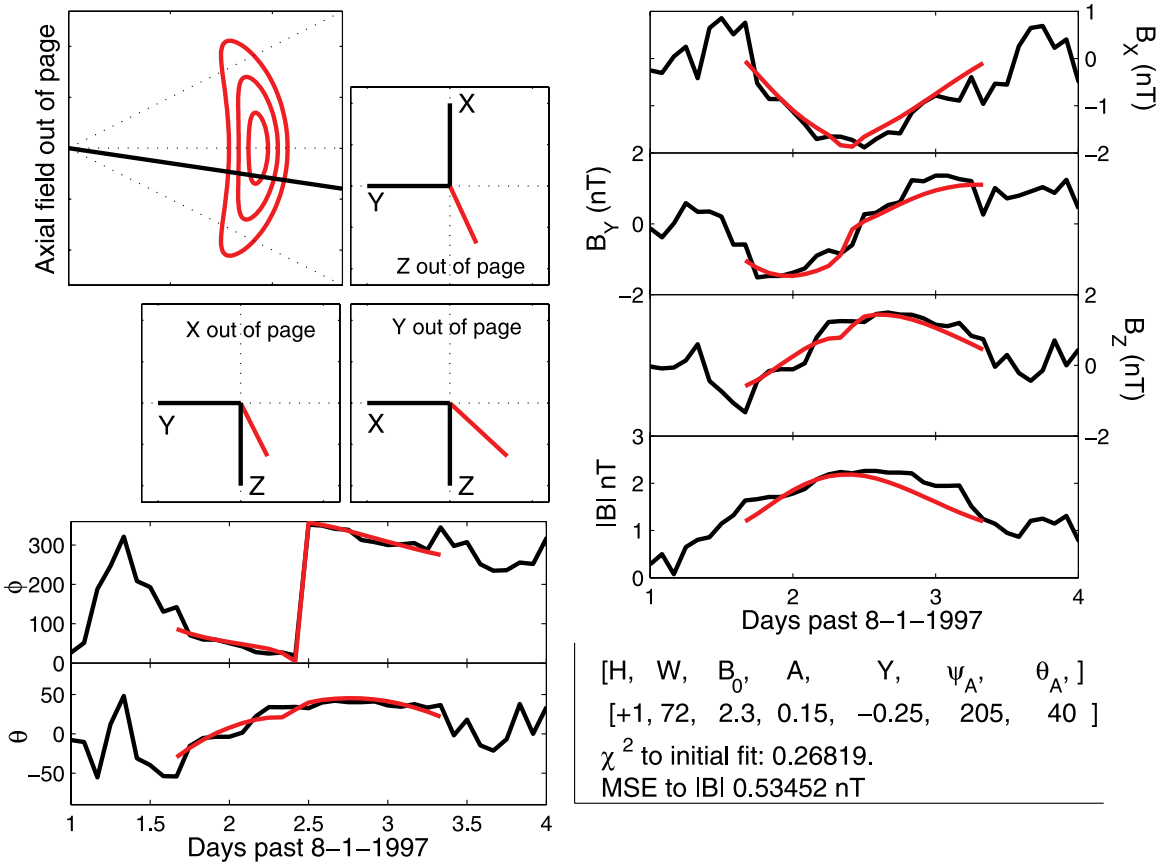

Figure 5. A summary of the magnetic cloud fit to the Ulysses observations of the January 1997 magnetic cloud, constrained using the LASCO estimate of the CME width. The top left panel shows the shape of the magnetic cloud cross-section. Surrounding it, the three smaller panels show the axis orientation: The flux rope axis is most closely aligned with the Z direction, although it also has a large $-X$ component. The bottom two panels on the left show the observed (black) and model (red) magnetic field angle time series, whereas the top four panels on the right show the magnetic field components and magnitude. The bottom right panel summarizes the parameters of the fit.

netic field angles, whereas the top four panels on the right show the magnetic field components and magnitude. The bottom right panel summarizes the parameters of the fit (also shown in Table 1). From the time-series comparison it can be seen that a good fit was obtained in terms of matching the in situ magnetic field measurements. The reconstructed flux rope axis lies mainly in the Z and $-X$ directions, i.e., lying almost in the plane of the sky from SOHO's vantage point. Ulysses appears to have intersected the flux rope approximately one quarter of the way through its cross section, measuring from the axis to the outer edge. Thus, assuming the leading edge of the magnetic cloud can be considered locally planar, the normal to the leading edge should point in $-X$, $+Y$, $-Z$ directions. This orientation is supported by both the orientations of the planar magnetic structuring and nonradial flow deflections in the sheath.

4. Discussion

[38] In situ observations, in isolation, are inadequate to estimate the nonradial extent of magnetic clouds: The magnetic field time series for a circular cross-section flux rope is almost indistinguishable from that of a flux rope with a highly elongated cross-section. For this reason, it is necessary to further constraining magnetic cloud reconstruction through the use of coronagraph observations of the CME widths. Observations of elliptical halo CMEs suggest the coronagraph-measured width of a limb CME may depend on the orientation of the associated flux rope [*Zhao*, 2008]: The coronagraph-measured width is the equal to the flux-rope cross-sectional width for ropes observed "edge-on" (i.e., with axes perpendicular to the plane of the sky), but these two parameters are not necessarily equal for ropes observed "side-on" (i.e., with axes in the plane of the sky). The small ellipticities typically observed for halo CMEs, however, suggest the error should be relatively small.

[39] A new technique for combined remote and in situ CME observations is outlined and applied to Ulysses-SOHO quadrature observations. This technique has obvious applications to the STEREO mission, once the spacecraft reach sufficient angular separation. In principle, however, it could also be routinely applied to nonquadrature observations, such as those regularly performed by the ACE/Wind and SOHO spacecraft, through the use of a cone model estimate of the width of a halo CME. At present it is unclear

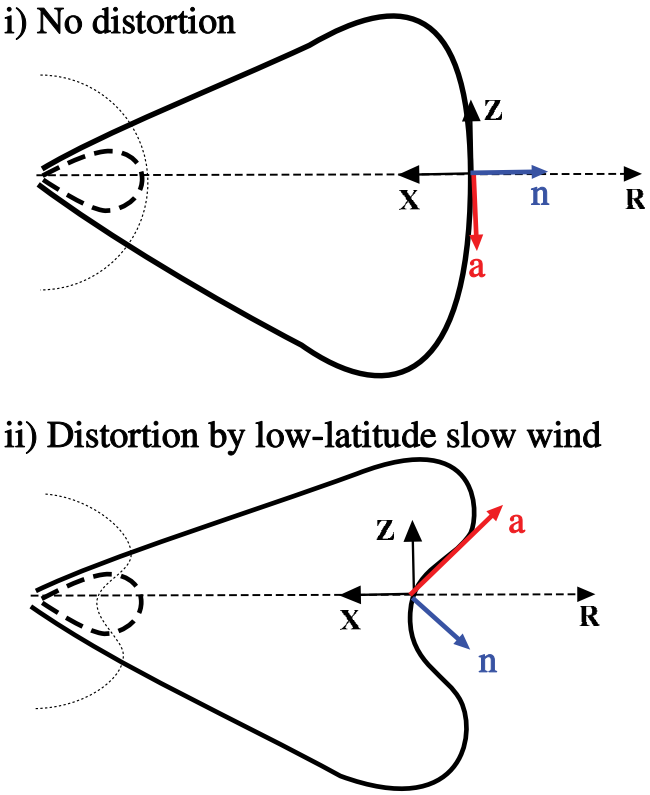

Figure 6. A sketch of the expected flux rope axis orientations in the plane of the sky, as viewed from LASCO. The dashed (solid) loops show the axis when the ejection is in the LASCO field of view (at Ulysses). The top shows distortion by a uniform ambient solar wind so that the axis of the flux rope at Ulysses, shown as a red arrow, is expected to be perpendicular to the radial direction. The bottom shows distortion from a low-latitude band of slow wind, such as would be expected at solar minimum. The local axis orientation would then be expected to have a significant radial component, as observed.

whether such cone model fits to halo CMEs are sufficiently accurate for this purpose.

4.1. Geometry of the December 1996 Ulysses-SOHO Quadrature Event

[40] The estimated axis orientation of the December 1996 Ulysses-SOHO quadrature event at 4.7 AU was similar for both force-free and kinematically distorted flux rope fits. The cross-sectional elongation, however was $\times 5$ greater for the new technique compared to the force-free approach, resulting in an axial flux content $\times 4$ larger. Fits to more events are required to determine whether this difference in flux is representative of the flux underestimate of the force-free flux rope technique.

[41] Strong evidence for distortion of the magnetic cloud resulting from interaction with the ambient solar wind was also found for this event. Figure 6 shows a sketch of the expected flux rope axis orientations in the plane of the sky, as viewed from LASCO. The dashed (solid) loops show the axis when the ejection is in the LASCO field of view (at Ulysses). The top shows flux rope distortion by a uniform ambient solar wind. With increasing radial distance, the leading edge of the flux rope should become increasingly aligned with a heliocentric circle [e.g.., *Riley and Crooker*, 2004]. By 5 AU, the deviation from a heliocentric circle should be $\sim 1\ R_S/5\text{AU} \sim 1/1000$, assuming an initial radius of curvature of 1 R_S close to the Sun. Thus, aside from at the extreme flanks of the flux rope where the flux rope signature may not be recognizable as a spacecraft would travel almost along the axis, the local axis orientation should exhibit a negligible radial component. The axis of the flux rope at Ulysses, shown as a red arrow, is therefore expected to be nearly perpendicular to the radial direction. The bottom of Figure 6 shows distortion from a low-latitude band of slow wind, such as would be expected at solar minimum, resulting in a concave-outward shape to the flux rope [e.g., *Odstrcil et al.*, 2004]. As the axis traces the center of the rope structure, the local axis orientation at Ulysses would then be expected to have a significant radial component, as is observed. The normal to the planar magnetic structures and the deflected flows in the sheath both agree with this interpretation. While distortion occurs along the axis, the good fit of the model to the observed time series suggests that the cross-section of the flux rope maintains its convex-outward shape, as little variation in ambient solar wind speed is expected perpendicular to the magnetic cloud axis.

[42] The event under study does not fully conform to the proposed explanation for structured/unstructured CMEs [*Cremades and Bothmer*, 2004]: They suggested that, statistically, east-limb CMEs should appear structured because of the flux-rope being observed "end-on", whereas west-limb CMEs should appear unstructured because of the flux rope lying in the plane of the sky. LASCO observations of the December 1996 west-limb CME show a highly structured event with a classic "light bulb" morphology, contrary to the [*Cremades and Bothmer*, 2004] trend. While the structured nature of the CME suggests a flux rope viewed "end-on", the associated ICME at 4.7 AU has a flux rope axis lying close to the plane of the sky. Thus this event is in agreement with the [*Cremades and Bothmer*, 2004] predicted flux-rope orientation for a west-limb CME, but contrary to their interpretation of a structured CME. At present, it is not clear whether the flux-rope has undergone rotation in interplanetary space [e.g., *Webb et al.*, 2000], or whether a structured CME does not indicate a flux rope is being viewed "edge-on". Observationally, these trends clearly merit further investigation with a much broader data set, whereas the feasibility of large-scale ejecta rotation resulting from interaction with solar wind structures may be best approached through numerical simulation.

4.2. Effect of Drag

[43] Flux-ropes of different cross-sectional width will present different obstacles to the ambient solar wind flow, resulting in different levels of drag and ultimately different propagation times. If the ambient solar wind conditions are known, propagation times could, in principle, be used to calculate the net drag forces acting on ejecta and hence infer information about their morphology, such as their cross-sectional extent. Analytically, however, this may not be feasible: The highly structured ambient solar wind means that not only does an ICME experience different levels of drag across its cross-sectional extent, but this drag gradient

results in distortion of the shape of the ICME shape, greatly complicating the calculation of a drag coefficient [*Cargill*, 2004; *Vršnak and Gopalswamy*, 2002]. This problem is therefore best addressed via numerical simulation. Initial MHD simulations of the propagation of ejecta through realistic ambient solar wind conditions suggest that the ambient solar wind may affect the propagation time as much as the initial speed of the CME [*Case et al.*, 2008]. These simulations, however, do not include a magnetic flux rope within the ejecta, instead providing excess pressure and density via an over-dense plasma blob. The effect of CME angular width could also be investigated in this way, but the errors and assumptions in simulating the ambient conditions and the internal structure of the ICME may outweigh any insight gained from the simulations.

4.3. Implications of Greater CME Magnetic Flux Content

[44] For the December 1996 CME, the magnetic flux content was found to be $\times 4$ greater than the force-free magnetic flux rope estimate. A higher typical CME flux content increases the amount of magnetic flux added to the heliosphere by CMEs over the solar cycle [*Owens et al.*, 2006; *Owens and Crooker*, 2006], requiring a lower background open flux and/or a reduction in the time for which CMEs contribute flux to the heliosphere than previously predicted in order to match the observed heliospheric magnetic field intensity. It is worth noting, however, the possibility that the magnetic flux content of magnetic clouds may not be representative of CMEs in general, and that as the fraction of ICMEs displaying a magnetic signature varies over the solar cycle [*Riley et al.*, 2006], so may the average CME magnetic flux content. Further modeling of such effects is required.

[45] **Acknowledgments.** This research was supported by the National Science Foundation Agreement ATM-012950, which funds the CISM project of the STC program, with additional support from NSF agreement ATM-0553397 and by the STFC (UK). I have benefited from the availability of Ulysses data (VHM/FGM PI: A. Balogh, and SWOOPS PI: D. McComas). The SOHO/LASCO data used here are produced by a consortium of the Naval Research Laboratory (USA), Max-Planck-Institut fuer Aeronomie (Germany), Laboratoire d'Astronomie (France), and the University of Birmingham (UK). SOHO is a project of international cooperation between ESA and NASA.

[46] Amitava Bhattacharjee thanks the reviewers for their assistance in evaluating this paper.

References

Burlaga, L. F. (1998), Magnetic clouds: Constant alpha force-free configurations, *J. Geophys. Res.*, *93*, 277–285.

Burlaga, L. F., E. Sittler, F. Mariani, and R. Schwenn (1981), Magnetic loop behind and interplanetary shock: Voyager, Helios, and IMP 8 observations, *J. Geophys. Res.*, *86*, 6673–6684.

Cargill, P. J. (2004), On the aerodynamic drag force acting on coronal mass ejections, *Sol. Phys.*, *221*, 135.

Case, A., H. E. Spence, M. J. Owens, P. Riley, and D. Odstrcil (2008), The ambient solar wind's effect on ICME transit times, *Geophys. Res. Lett.*, *35*, L15105, doi:10.1029/2008GL034493.

Cremades, H., and V. Bothmer (2004), On the three-dimensional configuration of coronal mass ejections, *Astron. Astrophys.*, *422*, 307–322, doi:10.1051/0004-6361:20035776.

Funsten, H. O., J. T. Gosling, P. Riley, O. C. S. Cyr, R. J. Forsyth, R. A. Howard, and R. Schwenn (1999), Combined Ulysses solar wind and SOHO coronal observations of several west limb coronal mass ejections, *J. Geophys. Res.*, *104*, 6679–6689.

Goldstein, H. (1983), On the field configuration in magnetic clouds, in *Solar Wind Conference*, edited by M. Neugebauer, pp. 731–733, NASA Conf. Publ.

Gosling, J. T., D. N. Baker, S. J. Bame, W. C. Feldman, and R. D. Zwickl (1987), Bidirectional solar wind electron heat flux events, *J. Geophys. Res.*, *92*, 8519–8535.

Harrison, R. A., et al. (2008), First imaging of coronal mass ejections in the heliosphere viewed from outside the Sun Earth line, *Sol. Phys.*, *247*, 171–193, doi:10.1007/s11207-007-9083-6.

Hidalgo, M. A., C. Cid, A. F. Vinas, and J. Sequeiros (2002), A non-force-free approach to the topology of magnetic clouds, *J. Geophys. Res.*, *107*(A1), 1002, doi:10.1029/2001JA900100.

Hu, Q., and B. U. O. Sonnerup (2001), Reconstruction of magnetic flux ropes in the solar wind, *Geophys. Res. Lett.*, *28*, 467–470.

Hundhausen, A. J. (1993), Sizes and locations of coronal mass ejections—SMM observations from 1980 and 1984–1989, *J. Geophys. Res.*, *98*, 13,177–13,200.

Jones, G. H., A. Rees, A. Balogh, and R. J. Forsyth (2002), The draping of heliospheric magnetic fields upstream of coronal mass ejecta, *Geophys. Res. Lett.*, *29*(11), 1520, doi:10.1029/2001GL014110.

Klein, L. W., and L. F. Burlaga (1982), Interplanetary magnetic clouds at 1 AU, *J. Geophys. Res.*, *87*, 613–624.

Lepping, R. P., J. A. Jones, and L. F. Burlaga (1990), Magnetic field structure of interplanetary clouds at 1 AU, *J. Geophys. Res.*, *95*, 11,957–11,965.

Lindsay, G. M., J. G. Luhmann, C. T. Russell, and J. T. Gosling (1999), Relationships between coronal mass ejection speeds from coronagraph images and interplanetary characteristics of associated interplanetary coronal mass ejections, *J. Geophys. Res.*, *104*, 12,515–12,523.

Lundquist, S. (1950), Magnetostatic fields, *Ark. Fys.*, *2*, 361–365.

Marubashi, K. (1997), Interplanetary magnetic flux ropes and solar filaments, in *Coronal Mass Ejections*, *Geophys. Monogr. Ser.*, vol. 99, edited by N. Crooker, J. Joselyn, and J. Feynman, p. 147, AGU, Washington.

McAllister, A. H., S. F. Martin, N. U. Crooker, R. P. Lepping, and R. J. Fitzenreiter (2001), A test of real-time prediction of magnetic cloud topology and geomagnetic storm occurrence from solar signatures, *J. Geophys. Res.*, *106*, 29,185–29,194.

Michalek, G., N. Gopalswamy, and S. Yashiro (2003), A new method for estimating widths, velocities, and source location of halo coronal mass ejections, *Astrophys. J.*, *584*, 472–478.

Mulligan, T., and C. T. Russell (2001), Mulitspacecraft modeling of the flux rope structure of interplanetary coronal mass ejections: Cylindrical symmetric versus nonsymmetric topologies, *J. Geophys. Res.*, *106*, 10,581–10,596.

Nakagawa, T., A. Nishida, and T. Saito (1989), Planar magnetic structures in the solar wind, *J. Geophys. Res.*, *94*, 11,761–11,775.

Odstrcil, D., P. Riley, and X.-P. Zhao (2004), Numerical simulation of the 12 May 1997 interplanetary CME event, *J. Geophys. Res.*, *109*, A02116, doi:10.1029/2003JA010135.

Owens, M. J. (2006), Magnetic cloud distortion resulting from propagation through a structured solar wind: Models and observations, *J. Geophys. Res.*, *111*, A12109, doi:10.1029/2006JA011903.

Owens, M. J., and P. J. Cargill (2004), Non-radial solar wind flows induced by the motion of interplanetary coronal mass ejections, *Ann. Geophys.*, *22*, 4397–4406.

Owens, M. J., and N. U. Crooker (2006), Coronal mass ejections and magnetic flux buildup in the heliosphere, *J. Geophys. Res.*, *111*, A10104, doi:10.1029/2006JA011641.

Owens, M. J., P. J. Cargill, C. Pagel, G. L. Siscoe, and N. U. Crooker (2005), Characteristic magnetic field and speed properties of interplanetary coronal mass ejections and their sheath regions, *J. Geophys. Res.*, *110*, A01105, doi:10.1029/2004JA010814.

Owens, M. J., V. G. Merkin, and P. Riley (2006), A kinematically distorted flux rope model for magnetic clouds, *J. Geophys. Res.*, *111*, A03104, doi:10.1029/2005JA011460.

Owens, M. J., N. A. Schwadron, N. U. Crooker, W. J. Hughes, and H. E. Spence (2007), Role of coronal mass ejections in the heliospheric Hale cycle, *Geophys. Res. Lett.*, *34*, L06104, doi:10.1029/2006GL028795.

Richardson, I. G., H. V. Cane, and E. W. Cliver (2002), Sources of geomagnetic activity during nearly three solar cycles (1972–2000), *J. Geophys. Res.*, *107*(A8), 1187, doi:10.1029/2001JA000504.

Riley, P., and N. U. Crooker (2004), Kinematic treatment of CME evolution in the solar wind, *Astrophys. J.*, *600*, 1035–1042.

Riley, P., et al. (2004), Fitting flux-ropes to a global MHD solution: A comparison of techniques, *J. Atmos. Sol.-Terr. Phys.*, *66*, 1321–1332.

Riley, P., C. Schatzman, H. V. Cane, I. G. Richardson, and N. Gopalswamy (2006), On the rates of coronal mass ejections: Remote solar and in situ observations, *Astrophys. J.*, *647*, 648–653.

Russell, C. T., and T. Mulligan (2002), On the magnetosheath thicknesses of interplanetary coronal mass ejections, *Planet. Space Sci.*, *50*, 527–534.

Schwenn, R., A. Dal Lago, E. Huttunen, and W. D. Gonzalez (2005), The association of coronal mass ejections with their effects near the Earth, *Ann. Geophys.*, *23*, 1033–1059.

Sonnerup, B. U. O., and L. J. Cahill (1967), Magnetopause structure and attitude from Explorer 12 observations, *J. Geophys. Res.*, *72*, 171–783.
St. Cyr., O. C., et al. (2000), Properties of coronal mass ejections: SOHO LASCO observations from January 1996 to June 1998, *J. Geophys. Res.*, *105*, 18,169–18,185.
Thompson, B. J., S. P. Plunkett, J. B. Gurman, J. S. Newmark, O. C. St. Cyr, and D. J. Michels (1998), SOHO/EIT observations of an Earth-directed coronal mass ejection on May 12, 1997, *Geophys. Res. Lett.*, *25*, 2465–2468.
Vršnak, B., and N. Gopalswamy (2002), Influence of aerodynamic drag on the motion of interplanetary ejecta, *J. Geophys. Res.*, *107*(A2), 1029, doi:10.1029/2001JA000120.
Wang, Y., G. Zhou, P. Ye, S. Wang, and J. Wang (2006), A study of the orientation of interplanetary magnetic clouds and solar filaments, *Astrophys. J.*, *651*, 1245–1255, doi:10.1086/507668.
Webb, D. F., R. P. Lepping, L. F. Burlaga, C. E. DeForest, D. E. Larson, S. F. Martin, S. P. Plunkett, and D. M. Rust (2000), The origin and development of the May 1997 magnetic cloud, *J. Geophys. Res.*, *105*, 27,251–27,259.
Wimmer-Schweingruber, R. F., et al. (2006), Understanding interplanetary coronal mass ejection signatures, *Space Sci. Rev.*, *123*, 177–216, doi:10.1007/s11214-006-9017-x.
Yashiro, S., N. Gopalswamy, S. Akiyama, G. Michalek, and R. A. Howard (2005), Visibility of coronal mass ejections as a function of flare location and intensity, *J. Geophys. Res.*, *110*, A12S05, doi:10.1029/2005JA011151.
Yurchyshyn, V. B., H. Wang, P. R. Goode, and Y. Deng (2001), Orientation of the magnetic fields in interplanetary flux ropes and solar filaments, *Astrophys. J.*, *563*, 381–388, doi:10.1086/323778.
Zhao, X. P. (2008), Inversion solutions of the elliptic cone model for disk frontside full halo coronal mass ejections, *J. Geophys. Res.*, *113*, A02101, doi:10.1029/2007JA012582.
Zhao, X.-P., S. P. Plunkett, and W. Liu (2002), Determination of geometrical and kinematical properties of halo coronal mass ejections using the cone model, *J. Geophys. Res.*, *107*(A8), 1223, doi:10.1029/2001JA009143.

M. J. Owens, Space and Atmospheric Physics, Blackett Laboratory, Imperial College London, Prince Consort Road, London SW7 2BZ, UK. (m.owens@imperial.ac.uk)